

# The Tin Pest Problem as a Test of Density Functionals Using High-Throughput Calculations

Michael J. Mehl,<sup>1,\*</sup> Mateo Ronquillo,<sup>2</sup> David Hicks,<sup>3</sup> Marco Esters,<sup>3</sup> Corey Oses,<sup>3</sup> Rico Friedrich,<sup>3</sup> Andriy Smolyanyuk,<sup>3</sup> Eric Gossett,<sup>3</sup> Daniel Finkenstadt,<sup>4</sup> and Stefano Curtarolo<sup>3,†</sup>

<sup>1</sup>*Center for Autonomous Materials Design, Duke University, Durham NC 27708*

<sup>2</sup>*U. S. Nuclear Power School, Goose Creek, South Carolina 29445*

<sup>3</sup>*Center of Autonomous Materials Design, Duke University, Durham NC 27708*

<sup>4</sup>*Physics Department, U.S. Naval Academy, Annapolis, Maryland 21402*

(Dated: January 22, 2022)

At ambient pressure tin transforms from its ground-state semi-metal  $\alpha$ -Sn (diamond structure) phase to the compact metallic  $\beta$ -Sn phase at 13°C (286K). There may be a further transition to the simple hexagonal  $\gamma$ -Sn above 450K. These relatively low transition temperatures are due to the small energy differences between the structures,  $\approx 20$  meV/atom between  $\alpha$ - and  $\beta$ -Sn. This makes tin an exceptionally sensitive test of the accuracy of density functionals and computational methods. Here we use the high-throughput Automatic-FLOW (AFLOW) method to study the energetics of tin in multiple structures using a variety of density functionals. We look at the successes and deficiencies of each functional. As no functional is completely satisfactory, we look Hubbard U corrections and show that the Coulomb interaction can be chosen to predict the correct phase transition temperature. We also discuss the necessity of testing high-throughput calculations for convergence for systems with small energy differences.

## I. INTRODUCTION

Tin is one of the few elements which undergoes a near-room-temperature (286K) first-order structural phase transition from semi-metallic  $\alpha$ -Sn (gray tin, diamond, *Strukturbericht* designation A4, AFLOW label [1] A\_cF8-227\_a) to metallic  $\beta$ -Sn (white tin, *Strukturbericht* designation A5, AFLOW label A\_tI4-141\_a).[2] This transition takes place slowly and is accompanied by a large (20%) reduction in the volume. On cooling the resulting expansion leads to the “tin-pest” problem when  $\beta$ -Sn is stored at low temperatures.[3] Consequences of this have occurred in the real world[4, 5] and in legend.[6] Today, the main concern about tin-pest is in lead-free solders,[7] as they seem to be more susceptible to the problem than the traditional tin-lead amalgam.

In addition to its well-known phases, tin may undergo a transition from  $\beta$ -Sn to  $\gamma$ -Sn at 450K.[8] This phase is said to be a slight orthorhombic distortion of the simple hexagonal lattice (*Strukturbericht* designation A<sub>f</sub>, Pearson symbol *hP1*, space group *P6/mmm*#191, AFLOW label A\_hP1-191\_a) a structure not observed at ambient pressure in any other element. It can be stabilized in the hexagonal  $\gamma$ -Sn form by alloying with cadmium, indium, lead and mercury.[9–11] Alloys such as In<sub>0.45</sub>Bi<sub>0.55</sub> are also found in this structure.[12]

The static lattice energy difference between  $\alpha$ - and  $\beta$ -Sn has not been directly determined by experiment, but it is estimated to be in the range 10-40 meV/atom.[13, 14] This makes the prediction of the  $\alpha$ -Sn  $\rightarrow$   $\beta$ -Sn transition difficult for density functional (DFT) calculations, which may not achieve the required accuracy.[13, 15–18]

In fact, as we shall see, different functionals will give different predictions for the  $\alpha \rightarrow \beta$  transition temperature, some will find  $\beta$ -Sn as the ground state, and others will predict the ground state of tin to be close-packed structure. Tin then becomes an ideal system for testing the accuracy of density functionals, including supposedly more accurate generalized-gradient (GGA) and meta-GGA functionals.

Since the tin phase transition is thermal, its prediction requires accurate static-lattice energy and vibrational spectra for the  $\alpha$ -,  $\beta$ -, and  $\gamma$ -Sn as well as static-lattice energies for the close-packed phases. This large number of calculations, involving supercells of up to 256 atoms, is best handled by high-throughput methods, but this introduces another source of error: the basis-set and k-point mesh sizes set by default in these programs might not be accurate enough to find the correct ordering of phases. Thorough testing of the predictive capability of different functionals also requires testing of convergence criteria in the programs that evaluate DFT energies.

In this paper we will test several DFTs, determining the static lattice energy of tin at multiple volumes in a variety of crystal structures, computing the corresponding phonon spectra for the  $\alpha$ -,  $\beta$ -, and  $\gamma$ -Sn phases, and evaluating the free energy for each structures as a function of temperature. These calculations are most easily accomplished via high-throughput calculations and we use the AFLOW (Automatic FLOW) platform[19–24], with the Vienna *Ab initio* Simulation Package (VASP) to perform the first-principles calculations,[25–28] allowing AFLOW set up, run, and interpret the calculations using its harmonic phonon module (APL)[29, 30].

Our strategy is to use AFLOW and VASP to look at possible elemental structures for tin using local, generalized-gradient, and meta-GGA density functionals available in VASP. We previously showed[31] that different functionals can predict quite different ground state

\*Electronic address: michael.mehl@duke.edu

†Electronic address: stefano@duke.edu

structures. Here a functional must predict that  $\alpha$ -Sn is the ground state of tin and that the  $\beta$ -Sn phase is close enough in energy to it that a room-temperature thermal phase transition is possible. If it is, we then compute the phonon spectra of these phases as a function of volume, use this to find the free energy as a function of temperature within the quasi-harmonic approximation, and determine the functional's prediction of the transition temperature.

Finally, we note that the default settings for high-throughput calculations need to be carefully checked in situations where there are small energy differences. Here we show that different choices of basis-sets and k-points meshes can give different results for the lowest energy structure.

The paper is organized as follows: computational details are provided in Section II. Section III describes the crystal structures investigated in this paper, including the many ways the structures are referred to in the literature. Section IV summarizes our results for the LDA, GGA, and meta-GGA density functionals available in VASP. Section V considers the thermal properties of the  $\alpha$ -,  $\beta$ -, and  $\gamma$ -Sn phases, including predictions of phase transition temperatures. In Section VI we apply a Hubbard correction to the LDA and PBE functionals to see if we can improve our results. In this we follow Legrain and Manzhos[18], using the VASP implementation of LDAU[32, 33] to determine the changes made by applying a Hubbard  $U$  to either the  $s$ - or  $p$ -valence orbitals in tin, and show that with one adjustable parameter we can correctly predict the 286K phase transition. Section VII discusses the problems of convergence in systems with small energy differences between phases. Finally, section VIII summarizes our results.

## II. COMPUTATIONAL DETAILS

All calculations were performed using the high-throughput AFLOW (Automatic FLOW)[19–21] framework, using Vienna *Ab initio* Simulation Package (VASP) version 5.4.4 to perform the first-principles calculations,[25–28] using the Projector Augmented-Wave (PAW) method[34, 35] with the standard VASP POTCAR files. Calculations with the Perdew-Burke-Ernzerhof (PBE) functional[36] used the VASP  $s^2p^2$  “Sn” PBE POTCAR (dated 08Apr2002). Local Density Approximation (LDA) and other GGAs used the corresponding LDA POTCAR (03Oct2001), with the appropriate choice of the GGA or METAGGA tag in the INCAR file. Meta-GGA functional calculations require kinetic energy information only available in POTCARs available starting with VASP 5.4, so for those we used the  $s^2p^2d^{10}$  LDA POTCAR (dated 09Feb1998). In general we used the AFLOW defaults for energy cutoffs and  $\Gamma$ -centered k-point meshes, with the exceptions noted below.

Phonon spectra, vibrational free energy, and the ther-

mal expansion of the  $\alpha$ -,  $\beta$ -, and simple hexagonal  $\gamma$ -Sn structures were done using the Automatic Phonon Library (APL) module in AFLOW. The phonon spectra of both  $\beta$ - and  $\gamma$ -Sn are extremely sensitive to the k-point mesh size, so we had to adjust the default settings in APL to get good results while not over-burdening our computational platforms.

- For  $\alpha$ -Sn we used the standard face-centered cubic lattice vectors. APL calculations used a  $5 \times 5 \times 5$  (250 atom) supercell and a  $2 \times 2 \times 2$   $\Gamma$ -centered k-point mesh, yielding 6 k-points in the irreducible part of the supercell's Brillouin zone.
- $\beta$ -Sn has a very small value for  $c/a$  ( $\approx 0.54$ ), which required some special handling. We used the primitive vectors

$$\begin{aligned}\vec{a}_1 &= a \hat{x} \\ \vec{a}_2 &= a \hat{y}, \text{ and} \\ \vec{a}_3 &= \frac{1}{2}a \hat{x} + \frac{1}{2}a \hat{y} + \frac{1}{2}c \hat{z}\end{aligned}\quad (1)$$

for the body-centered-tetragonal primitive vectors. APL calculations used a  $4 \times 4 \times 8$  (256 atom) supercell, corresponding to a nearly-cubic  $4a \times 4a \times 4c$  tetragonal cell. A  $2 \times 2 \times 2$   $\Gamma$ -centered k-point mesh was chosen, yielding 8 k-points in the irreducible part of the supercell's Brillouin zone.

- We used a  $6 \times 6 \times 6$  (216 atom) supercell for the APL calculations for  $\gamma$ -Sn. The phonon spectra for this structure was extremely sensitive to the choice of k-point mesh, and we finally settled on a  $6 \times 6 \times 4$   $\Gamma$ -centered mesh with 47 k-points in the irreducible part of the supercell's Brillouin zone.

For a given primitive cell volume ( $V$ ) we calculated the free energy as a function of temperature for  $\alpha$ -,  $\beta$ - and  $\gamma$ -Sn by starting with the energy determined from the static lattice,  $U(V)$ . The AFLOW APL module then determine the phonon spectrum at this volume as well as the temperature-dependent vibrational energy  $U_{ph}(V, T)$  and entropy  $S_{ph}(V, T)$ . The free energy of the system at temperature  $T$  is given by:

$$F(V, T) = U(V) + U_{ph}(V, T) - T S_{ph}(V, T). \quad (2)$$

$U(V)$ ,  $U_{ph}(V, T)$  and  $S_{ph}(V, T)$  were computed for a number of volumes  $V_n$  around the equilibrium point. At a given temperature the minimum free-energy  $F(T)$  was determined by fitting the points  $F(V_n, T)$  to the third-order Birch equation of state[37] in the form[38]

$$\begin{aligned}F(V) &= F_0(T) + \frac{9}{8}K_0(T)V_0(T) \left[ \left( \frac{V_0(T)}{V} \right)^{2/3} - 1 \right]^2 \\ &+ \frac{9}{16}K_0(T)V_0(T)(K_0(T)' - 4) \left[ \left( \frac{V_0(T)}{V} \right)^{2/3} - 1 \right]^3\end{aligned}$$

where  $V_0$  is the equilibrium volume,  $F_0$  the equilibrium free energy,  $K_0$  the equilibrium bulk modulus, and  $K'_0$  the pressure derivative of the bulk modulus at equilibrium. The value  $F_0(T)$  in this calculation was taken to be the true free energy at the given temperature, and the associated volume,  $V_0(T)$ , can be used to compute the thermal expansion of the system and compare it with experiment.

While we only need the primitive cell volume  $V$  to completely specify the structure of  $\alpha$ -Sn, the  $\beta$ - and  $\gamma$ -Sn phases require that we also know the value of  $c/a$ , the ratio the lattice constant in the  $z$  direction compared to the lattice constant in the  $x - y$  plane. This means that a static lattice calculation will determine an energy  $U(V, c/a)$ . Fixing  $V$  and finding the minimum energy as a function of  $c/a$  will determine the energy  $U(V)$  at that volume. As the value of  $c/a$  which minimizes (2) can change with temperature, properly we should compute it as a function of  $V, c/a$ , and  $T$ , and determined the free energy by minimizing (2) in both  $V$  and  $c/a$  at fixed  $T$ . In practice the change in  $c/a$  with volume is so small during thermal expansion that this is not necessary, so we used the value of  $c/a$  determined by the static VASP calculation at all temperatures.

Visualizing and analyzing this data was accomplished using third-party software. In particular,

- The crystal structures shown in the next section were plotted using Jmol.[39]
- Phonon calculations in APL were checked comparing the phonon frequencies at selected wavelengths along high symmetry lines in the Brillouin zone with the frequencies computed by the frozen-phonon code FROZSL[40] at the same point. This helped us to determine the appropriate supercell k-point mesh for the simple hexagonal  $\gamma$ -Sn calculations.
- Some of the experimental phonon frequencies appearing in the figures were taken from published graphs. We used the Engauge Digitizer[41] to convert this data into a form we could use. Any errors in the process are ours.

### III. CRYSTAL STRUCTURES

We determined the static lattice energy/volume behavior  $U(V)$  for tin using many of the crystal structures observed in the group-IV elements as well as some close-packed and nearly close-packed elemental structures. As there are many notations for these structures it is useful to describe them here:

- The common names of the structures (*e.g.*, fcc, bcc, diamond or  $\alpha$ -Sn,  $\beta$ -Sn, simple hexagonal or  $\gamma$ -Sn, *etc.*).
- Elemental structures are most easily described by their *Strukturbericht* designations, as given in the

original works published by Ewald *et al.*,[42] or the extensions proposed by Smithells.[43] The exception here is Lonsdaleite,[44] hexagonal diamond, which has no *Strukturbericht* entry. We will primarily use the *Strukturbericht* labels in graphs to avoid clutter.

- For high-throughput calculations it is useful to have a label which allows the user to compactly specify the structure. Since we are using AFLOW, we use the AFLOW prototype label,[1] which uniquely specifies the stoichiometry, space group, and Wyckoff positions of the structure. Thus the diamond (A4,  $\alpha$ -Sn) structure is denoted A\_cF8.227\_a, denoting one type of atom (A), a face-centered cubic primitive cell with eight atoms in the conventional cell (Pearson symbol cF8), in space group #227 ( $Fd\bar{3}m$ ) with the atoms at the (8a) Wyckoff position.

More details about the structures, including the above information and a full description of the primitive lattice vectors and basis vectors can be found in the Library of Crystallographic Prototypes,[1, 45] available online at <http://www.aflow.org/prototype-encyclopedia>. The Library also allows the user to generate structure files for use as input in a wide variety of electronic structure codes, including the POSCAR files for these AFLOW/VASP calculations.

Table I describes all of the structures used here, including the common name, *Strukturbericht* label, space group, AFLOW prototype, and a link to the corresponding entry in the Library of crystallographic prototypes.

The face-centered cubic (A1), body-centered cubic (A2), and both body-centered tetragonal structures (A6,  $A_a$ ) can all be derived from one another by stretching or compressing the primitive cell along the (001) direction, with the A6 structure having a  $c/a$  ratio close to the A1 structure, and  $A_a$  near A2.

The structures of most interest in this work are  $\alpha$ -Sn (diamond structure, gray tin, or A4),  $\beta$ -Sn (white tin or A5) and simple hexagonal  $\gamma$ -Sn ( $A_f$ ) structures. These are shown in Figure 1. The  $\beta$ -Sn structure can be obtained from  $\alpha$ -Sn by compressing along the (001) axis of the diamond crystal. A possible transition path from  $\beta$ -Sn to  $\gamma$ -Sn was found by Needs and Martin.[46]

#### A. The $\gamma$ -Sn structure

While the  $\alpha$ - and  $\beta$ -Sn structures are well known, the  $\gamma$ -Sn structure is not. Smithells,[43] apparently referencing Raynor and Lee,[47] designated  $\text{HgSn}_{10}$  as the prototype for *Strukturbericht* designation  $A_f$ , with hexagonal space group  $P6/mmm$  #191 and one atom per unit cell located at the (1a) Wyckoff position. This can only be achieved if the mercury and tin atoms are randomly placed on the (1a) site. Alloys of tin with 5-20% of cadmium, indium, lead and mercury also exhibit this struc-

TABLE I: The elemental crystal structures investigated in this paper. As Lonsdaleite does not have a *Strukturbericht* designation we abbreviate it as “Lons.”

Common Name	<i>Strukturbericht</i>	Atoms/Cell	Space Group	AFLOW prototype
fcc (face-centered cubic)	A1	1	$Fm\bar{3}m$ #225	A_cF4_225_a
bcc (body-centered cubic)	A2	1	$Im\bar{3}m$ #229	A_cI2_229_a
hcp (hexagonal close-packed)	A3	2	$P6_3/mmc$ #194	A_hP2_194_c
diamond ( $\alpha$ -Sn)	A4	2	$Fd\bar{3}m$ #227	A_cF8_227_a
$\beta$ -Sn	A5	2	$I4_1/amd$ #141	A_tI4_141_a
In (body-centered tetragonal)	A6	1	$I4/mmm$ #139	A_tI2_139_a.In
$\alpha$ -Pr (body-centered tetragonal)	A <sub>a</sub>	1	$I4/mmm$ #139	A_tI2_139_a.alpha-Pa
$\gamma$ -Sn (simple hexagonal)	A <sub>f</sub>	1	$P6/mmm$ #191	A_hP1_191_a
sc (simple cubic)	A <sub>h</sub>	1	$Pm\bar{3}m$ #221	A_cP1_221_a
Lonsdaleite (hexagonal diamond)	Lons	4	$P6_3/mmc$ #194	A_hP4_194_f

ture, which is generally referred to as the  $\gamma$ -phase.[9–11] Parthé *et al.*[12] also list  $\text{In}_{0.45}\text{Bi}_{0.55}$  under the  $A_f$  designation.

Though it is not the ground state of any element, the simple hexagonal phase ( $\gamma$ -Sn) is observed at high pressures in silicon[46] and germanium.[48] When studying this phase it was found[46] that the simplest possible transition between  $\beta$ -Sn and  $\gamma$ -Sn is described by distorting either of the phases into a body-centered orthorhombic crystal, space group  $Imma$  #74, with the atoms at the (4e) Wyckoff position. This “Needs-Martin” path can be described using a body-centered orthorhombic unit cell, space group  $Imma$ #74, with atoms occupying the (4e) Wyckoff positions, locating the atoms at

$$\vec{b}_{\pm} = \pm(1/4b\hat{y} + zc\hat{z}) . \quad (4)$$

When  $a = b$  and  $z = 1/8$  this becomes the  $\beta$ -Sn structure. The  $\gamma$ -Sn structure is reached when  $z = 1/4$ ,  $a = 2c_{hex}$ ,  $b = \sqrt{3}a_{hex}$ , and  $c = a_{hex}$ , where  $a_{hex}$  and  $c_{hex}$  are the lattice constants of the hexagonal structure. Note that in this case the primitive cell contains two of the hexagonal primitive cells. This gives us a simple path to study the  $\alpha$ -Sn  $\leftrightarrow$   $\beta$ -Sn  $\leftrightarrow$   $\gamma$ -Sn transitions.

An elemental  $\gamma$ -Sn phase, occurring above 435K, was apparently described in texts around 1960, “but it is no longer referenced.”[8] In 1985 Kubiak[8] found that a structure he called the  $\gamma$  phase appeared after heating single crystal  $\beta$ -Sn in air at 450K for one week. He described this structure as having space group  $Cmmm$  #65, with two atoms in the conventional orthorhombic cell located on the (2a) Wyckoff position, and lattice parameters  $(a, b, c) = (5.8308 \text{ \AA}, 3.181 \text{ \AA}, 2.9154 \text{ \AA})$ . This structure is extremely close to simple hexagonal  $A_f$ , and when we run electronic structure calculations starting with Kubiak’s  $\gamma$ -Sn structure it always relaxes to the simple hexagonal  $A_f$  structure. Given this we will only consider the hexagonal structure in our calculations below, and refer to it as both  $\gamma$ -Sn and  $A_f$ .

The  $\gamma$ -Sn phase has been studied by Wehinger *et al.*,[49] who found that it was energetically similar to  $\beta$ -Sn using the LDA. They did not address its thermal

behavior, nor did they discuss the relationship of the two high-temperature phases with the ground state  $\alpha$ -Sn structure.

The orthorhombic elemental  $\gamma$ -Sn phase also can be stabilized in tin nanoparticles and nanowires.[50] We will not address this work here.

#### IV. DENSITY FUNCTIONALS USED TO STUDY TIN

In our study of the tungsten-nitrogen system[31] we found that the predicted ground state structure of a compound can change with the choice of density functional. Given the small energy difference between tin phases it is quite possible that different functionals will give different ground state structures. In this section we look at possible structures of tin with a variety of density functionals, all available in VASP:

- The Local Density Approximation (LDA),[51–53] which derives the Kohn-Sham potential[54] at a given point in space using only the charge density at that point. This is well-known to underestimate equilibrium lattice volumes.
- Generalized-Gradient Approximation (GGA) functionals, where the Kohn-Sham potential depends on the local charge density and its local gradient. These include
  - Perdew-Burke-Ernzerhof (PBE),[36] perhaps the most widely used GGA. This generally overestimates equilibrium lattice volumes.
  - Perdew-Burke-Ernzerhof revised for solids (PBEsol),[55] a modification of PBE optimized for solids rather than atoms.
  - Armiento-Mattsson (AM05),[56] designed to describe surfaces, but which has proved to be very accurate for solids.[57]

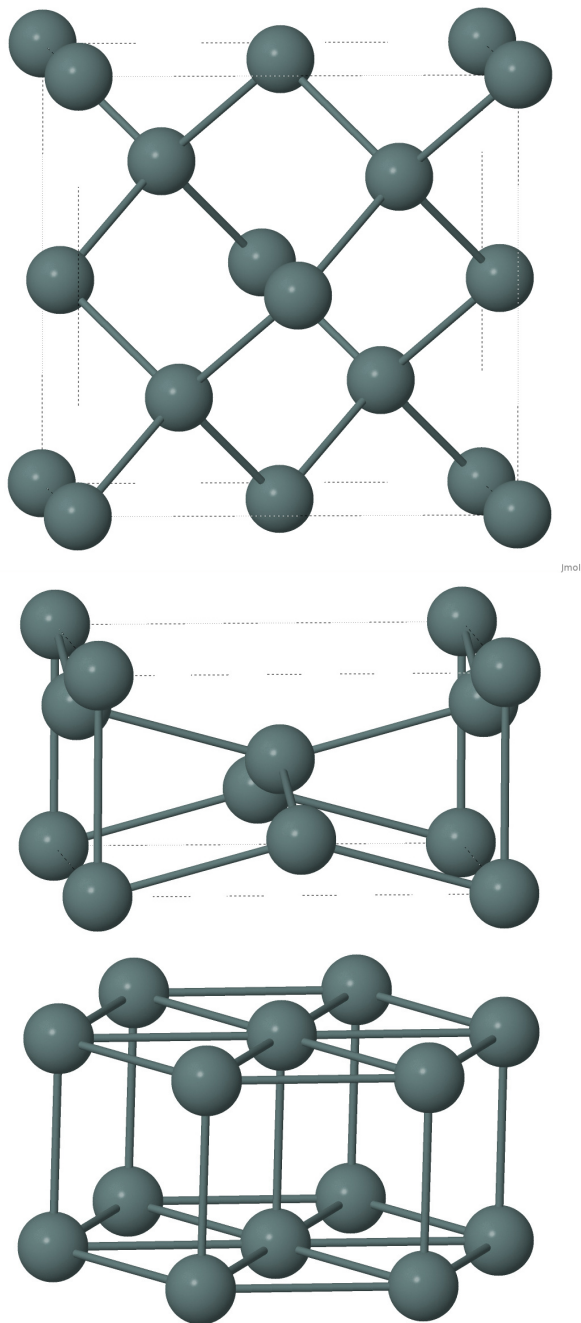


FIG. 1: The three low-energy structures of tin, drawn approximately to scale. Top:  $\alpha$ -Sn, *Strukturbericht* A4 (gray tin, diamond structure), AFLOW Designation A\_cF8\_227\_a. Middle:  $\beta$ -Sn, *Strukturbericht* A5 (white tin), AFLOW Designation A\_tI4\_141\_a. Bottom: simple hexagonal  $\gamma$ -Sn, *Strukturbericht* A<sub>f</sub>, AFLOW Designation A\_hP1\_191\_a. The conventional cells are shown for the cubic  $\alpha$ -Sn and tetragonal  $\beta$ -Sn. The  $\gamma$ -Sn figure contains three primitive cells to show the hexagonal structure.

- Meta-GGA functionals, which depend on the orbital kinetic energy density as well as the charge density and its gradient. VASP provides
  - Tao-Perdew-Staroverov-Scusera (TPSS),[58] designed to be correct for one- and two-electron systems and systems with slowly varying charge densities.
  - “Revised” TPSS (revTPSS),[59] which includes the second-order gradient expansion for exchange.
  - “Made-simple” functionals (MS0, MS1, MS2),[60, 61] which have empirical parameters.
  - M06-L,[62] optimized for main-group and transition metal chemistry.
  - “Strongly Constrained and Appropriately Normed” (SCAN),[63] which satisfies all known constraints on the exact density functional with no adjustable parameters. Since the SCAN functional properly describes both covalent and metallic bonding in silicon,[64] it should be able to describe similar behavior in tin.

These functionals have been tested over a variety of datasets,[57, 65, 66] but to our knowledge no test has been made on the accuracy of any of these functionals in describing the tin phase transition.

The remainder of this section discusses the behavior of tin as predicted by high-throughput calculations using the functionals described above. We first look at the energy-volume curves for tin in the phases described in Section III and Table I. If a functional appears to give a reasonable description of the behavior of tin we will look at its predictions of tin’s thermal expansion and the  $\alpha$ - $\beta$  transition in Section V.

#### A. The Local Density Approximation (LDA)

The energy-volume curves predicted by the Local Density Approximation (LDA) are shown in Figure 2.

As is usual with the LDA the predicted equilibrium volume for  $\beta$ -Sn is about 4% below the experimental volume. Somewhat surprisingly the equilibrium volume for  $\alpha$ -Sn is approximately equal to the low-temperature experimental volume.

As one expects there is a large equilibrium volume difference between  $\alpha$ - and  $\beta$ -Sn, in agreement with experiment. Lonsdaleite (“Lons.” in the figure), the hexagonal diamond structure, is correctly above  $\alpha$ -Sn (A4), and  $\gamma$ -Sn (A<sub>f</sub>) is above  $\beta$ -Sn (A5). We see that the LDA overbinds both  $\beta$ -Sn and  $\gamma$ -Sn with respect to  $\alpha$ -Sn, contrary to experiment, predicting a  $\beta$ -Sn ground state. In addition,  $\gamma$ -Sn is nearly degenerate with  $\beta$ -Sn, which, while not completely ruled out by experiment seems somewhat unlikely.

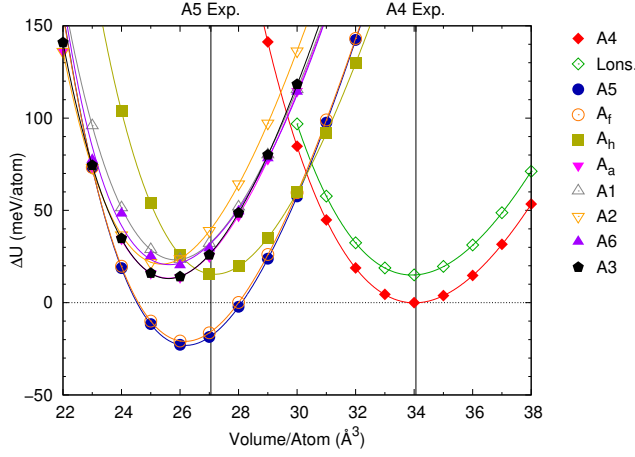


FIG. 2: Static lattice energy-volume curves for the tin structures discussed in Section III as predicted by AFLOW/VASP using the LDA functional. Structural notation is from Table I. We plot  $\Delta U$ , the change in energy per atom compared to the equilibrium energy of the  $\alpha$ -Sn ( $A_4$ ) structure. The lines labeled “A5 Exp.” and “A4 Exp.” represent the experimental volume of  $\beta$ -Sn ( $A_5$ ) at 298K[67] and  $\alpha$ -Sn ( $A_4$ ) at 90K[68] respectively.

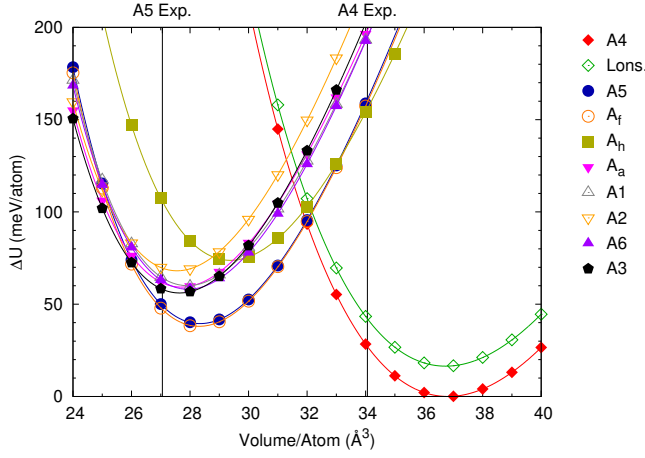


FIG. 3: Static lattice energy-volume curves for the tin structures discussed in Section III as predicted by AFLOW/VASP using the PBE functional. The notation is identical to that in Figure 2.

The prediction of  $\beta$ -Sn as the ground state within the LDA was also observed by Christensen and Methfessel[69] using the LMTO-ASA method. They found an equilibrium energy difference of 5 meV/atom, substantially less than our value of 20 meV/atom, but in neither case will we get the experimentally observed thermal transition.

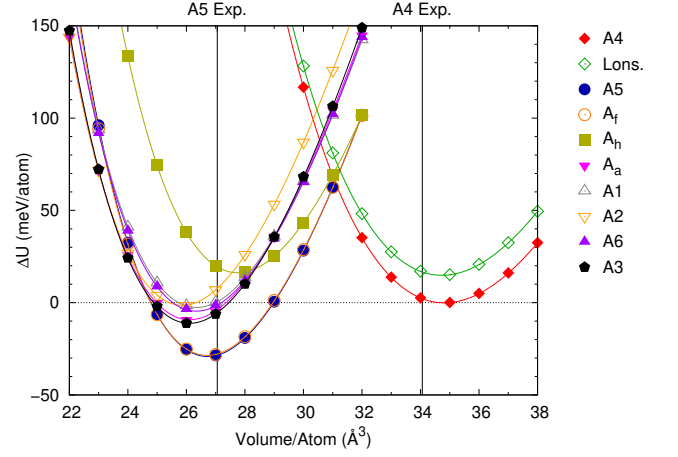


FIG. 4: Static lattice energy-volume curves for the tin structures discussed in Section III as predicted by AFLOW/VASP using the PBEsol functional. The notation is identical to that in Figure 2.

### B. The Perdew-Burke-Ernzerhof Generalized Gradient Functional (PBE)

The results for the PBE functional are shown in Figure 3. As is usual with the PBE, the predicted equilibrium volumes are 3-10% above the experimental values.

The PBE is an improvement over LDA in that it predicts that the equilibrium energy of the  $\beta$ -Sn phase is 40 meV above the  $\alpha$ -Sn, in agreement with previous work.[17] As with LDA, the  $\beta$ - and  $\gamma$ -Sn phases are nearly degenerate, but in the PBE the  $\gamma$ -phase is actually lower in energy than the  $\beta$ -Sn. Since  $\gamma$ -Sn is only observed at 450K and above (if at all), this is either an error of the PBE or the  $\beta$ -Sn phase must be stabilized by vibrational effects.

### C. The Perdew-Burke-Ernzerhof Generalized Gradient Functional Revised for Solids (PBEsol)

The results for the PBEsol functional are shown in Figure 4. Since this functional was designed to give better equilibrium volumes than PBE, it is not surprising that the equilibrium volumes for the  $\alpha$ -,  $\beta$ -, and  $\gamma$ - phases are between those predicted by the LDA and PBE functionals.

In other respects the PBEsol results are slightly worse than those found by the LDA. The  $\beta$ -Sn phase is even more bound compared to the  $\alpha$ - phase, and the  $\beta$ - and  $\gamma$ - phases are closer together and nearly indistinguishable on the plot.

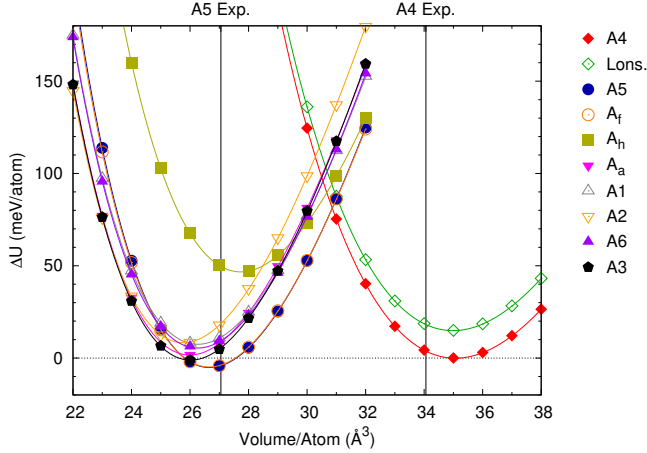


FIG. 5: Static lattice energy-volume curves for for the tin structures discussed in Section III as predicted by AFLOW/VASP using the AM05 functional. The notation is identical to that in Figure 2.

#### D. The Armiento-Mattsson Generalized Gradient Functional (AM05)

The results for the AM05 functional are shown in Figure 5. The equilibrium properties are similar to PBEsol, except that the  $\beta$ - and  $\gamma$ -Sn phases are less weakly bound compared to diamond than they are in LDA or PBEsol calculations.

It is interesting to look at the predictions for the close-packed (A1, A3) and near close-packed (A2, A6,  $A_a$ ) phases in this study. The previous functionals predicted that these phases had minimum energies 20-40 meV/atom above  $\beta$ - and  $\gamma$ -Sn. Here the energy difference is only about 5 meV/atom. This small energy difference leads to a prediction of a transition from  $\beta$ -Sn to body-centered cubic Sn at 1 GPa, far below the observed experimental transition at 35 GPa.[70]

#### E. Meta-GGA Functionals (except SCAN)

All of the meta-GGA functionals (TPSS, revTPSS, MS0/1/2, M06-L), with the exception of the SCAN functional discussed below, significantly overbind the close-packed fcc (A1) and hcp (A3) structures, as well as the nearly close-packed bcc (A2) structure compared to  $\alpha$ -,  $\beta$ -, and  $\gamma$ -Sn. Calculations using these functionals are significantly more time-consuming than LDA or GGA calculations, so once we realized this, we screened the functionals by looking at the energy difference between the hcp (A3) and  $\alpha$ -Sn (A4) phases. We did look at most of our target structures with the revTPSS functional, and show these results in Figure 6.

These functionals have been optimized for non-covalent interactions[62] so it is not surprising that they do not describe the energetics of the covalently-bonded  $\alpha$ -Sn phase

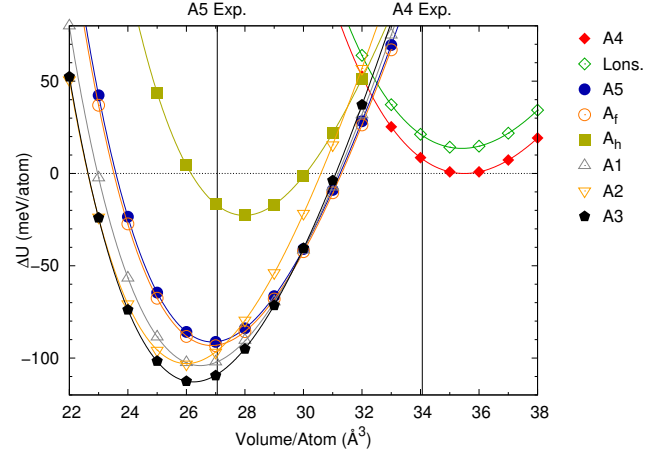


FIG. 6: Static lattice energy-volume curves for for most of the tin structures discussed in Section III as predicted by AFLOW/VASP using the revTPSS functional. The notation is identical to that in Figure 2. We did not do all of the structures in for this or the other non-SCAN meta-GGAs because of the time involved in the calculations. All of the non-SCAN meta-GGAs listed in Section IV significantly overbind the close-packed phases with respect to  $\alpha$ -,  $\beta$ -, and  $\gamma$ -Sn.

particularly well.

#### F. The Strongly Constrained and Appropriately Normed (SCAN) meta-GGA

Unlike meta-GGAs such as M06-L, the SCAN functional is non-empirical and is designed “to satisfy all 17 exact constraints appropriate to a semilocal functional.”[64] As shown in Figure 7, SCAN predicts the correct ordering of the major tin phases,  $U(\alpha\text{-Sn}) < U(\beta\text{-Sn}) < U(\gamma\text{-Sn})$ . The simple cubic ( $A_h$ ) phase is very low compared to other calculations, while the close-packed and nearly close-packed phases barely make the graph, with only the body-centered tetragonal  $\alpha$ -Pr ( $A_a$ ) phase within 200 meV of  $\alpha$ -Sn.

Table II provides a brief summary of the equilibrium properties of the three tin phase for each choice of DFT, along with the static energy difference between the three phases. The SCAN functional is the only one which correctly predicts the energy relationship  $U(\alpha\text{-Sn}) < U(\beta\text{-Sn}) < U(\gamma\text{-Sn})$ . In that sense it is better than any of the other functionals studied. Unfortunately the relative energy  $U(\beta\text{-Sn}) - U(\alpha\text{-Sn})$  is approximately 80 meV/atom, significantly larger than the 10-40 meV/atom suggested by the 286K transition temperature,[13, 14] and like most of the functionals discussed here it overestimates the equilibrium volumes for both gray and white tin.



TABLE II: Predicted equilibrium properties of  $\alpha$ -,  $\beta$ -, and  $\gamma$ -Sn for the density functionals described in Section IV, as well as the LDAU calculations described in Section VI. These calculations were made by allowing VASP to fully relax each unit cell, so the equilibrium volumes and energies will differ slightly from the Birch fit derived quantities used elsewhere in this paper.  $\Delta U_{\alpha\beta}$  and  $\Delta U_{\alpha\gamma}$  represent the equilibrium energy difference between  $\beta$ -Sn or  $\gamma$ -Sn and  $\alpha$ -Sn, respectively. A positive number indicates that  $\alpha$ -Sn is lower in energy. We also include experimentally measured lattice constants for comparison. The experimental lattice constants for  $\gamma$ -Sn are for the alloy with stoichiometry  $\text{Sn}_{0.8}\text{In}_{0.2}$ . [10]

	$\alpha$ -Sn a (Å)	$\beta$ -Sn a (Å)	$\beta$ -Sn c (Å)	$\gamma$ -Sn a (Å)	$\gamma$ -Sn c (Å)	$\Delta U_{\alpha\beta}$ (eV/atom)	$\Delta U_{\alpha\gamma}$ (eV/atom)
Exp. (90K)	6.483[68]						
Exp. (100K)		5.815[71]	3.164[71]				
Exp. (296K)	6.491[15]	5.832[71]	3.183[71]	3.216[10]	2.998[10]		
Exp. (300K)		5.3815[72]	3.1828[72]				
LDA	6.4787	5.7823	3.1325	3.1822	2.9844	-0.023	-0.021
PBE	6.6528	5.9334	3.2187	3.2645	3.0678	0.040	0.039
PBEsol	6.5296	5.8193	3.1550	3.2024	3.0052	-0.029	-0.029
AM05	6.5453	5.8135	3.1554	3.2000	3.0030	-0.005	-0.005
revTPSS	6.5501	5.8124	3.1502	3.1962	3.0034	-0.092	-0.094
SCAN	6.4235	5.7286	3.1116	3.1572	2.9551	0.081	0.086
LDA (LDAU, $U_p = -0.80$ )	6.4235	5.7286	3.1116	3.1572	2.9551	0.020	0.028
PBE (LDAU, $U_p = 0.20$ )	6.6751	5.9541	3.2271	3.2733	3.0805	0.025	0.022

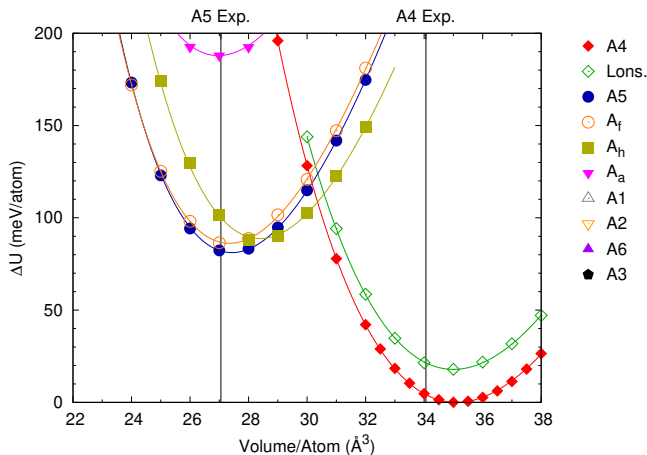


FIG. 7: Static lattice energy-volume curves for the tin structures discussed in Section III as predicted by AFLOW/VASP using the SCAN functional. The notation is identical to that in Figure 2. Structures not shown (A1, A2, A3, A6) are above the  $\Delta U = 200$  meV/atom limit of the graph.

## V. PHONONS AND THERMODYNAMICS

Of all the density functionals studied in Section IV, only two predict the  $\beta$ -Sn phase to have a higher energy than the  $\alpha$ -Sn phase: PBE and SCAN. The PBE functional has the apparent deficiency that the  $\gamma$ -Sn phase is lower in energy than the  $\beta$ -phase, but the energy difference is small and perhaps zero-point and/or thermal effects will stabilize  $\beta$ -Sn at finite temperatures. The AFLOW APL module allows us to determine the zero-

point and temperature-dependent free energy for all three of the tin phases. We will begin with the PBE functional. The procedure is as follows:

- Determine the total energy of the three possible phases of tin as a function of volume using AFLOW/VASP.
- Use the harmonic phonon module (APL) of AFLOW to determine the phonon spectra for each structure and volume.
- The APL module automatically determines the vibrational free energy (2) as a function of temperature for each of these structures and volumes, including the zero-point energy. Since the variation of  $c/a$  for the  $\beta$ - and  $\gamma$ -phases is small, we will ignore change in  $c/a$  with temperature and use the  $c/a$  found to minimize the static energy at each volume for all temperatures at the volume.
- For a given temperature, determine the volume which minimizes the free energy using the Birch fit (3), generating the free energy  $F(T)$  and equilibrium volume  $V(T)$ .
- Determine the averaged linear expansion coefficient of each structure using the relationship

$$\alpha(T) = \frac{1}{3V(T)} \frac{dV}{dT}(T), \quad (5)$$

where  $a(T)$  is the lattice constant of the crystal. For the tetragonal  $\beta$ - and hexagonal  $\gamma$ -phases  $\alpha(T)$  will be the average of the linear expansion coefficients in the  $x$ -,  $y$ -, and  $z$ -directions.



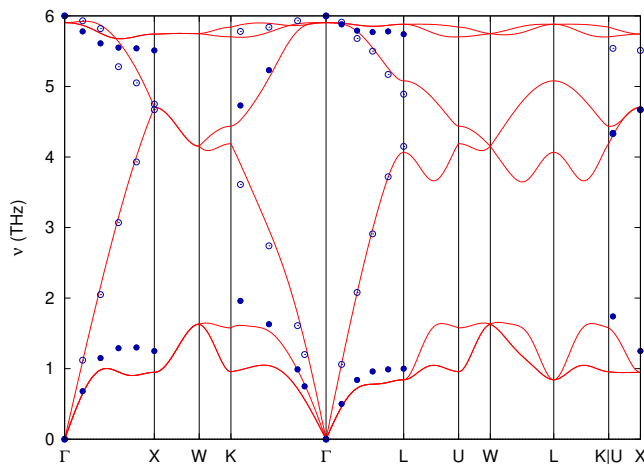


FIG. 8: Transverse (solid circles) and longitudinal (open circles) phonon frequencies for  $\alpha$ -Sn measured at 90K by Price *et al.*,[68] compared to the PBE phonon spectra at the primitive cell volume of  $68\text{\AA}^3$  calculated using the APL module of AFLOW. The high-symmetry paths through the face-centered cubic Brillouin zone are defined by Setyawan and Curtarolo.[73] Note that Price *et al.* only determined the frequencies of one of the transverse branches along the  $\Gamma - K$  and  $U - X$  directions (the  $\Sigma$  line).

- Compare the values of the free energy  $F(T)$  for each structure to determine the equilibrium structure as a function of temperature.

### A. Phonon Spectra

We must first ask if the APL module correctly describes the vibrational behavior of tin. Fortunately experimental phonon spectra for all three phases are available.

Phonon data for  $\alpha$ -Sn (gray tin, *Strukturbericht* A4) was obtained by Price *et al.*[68] at 90K, with a unit cell volume of  $68.1\text{\AA}^3$ . Our closest volume was  $68\text{\AA}^3$ , and we compare our results with theirs along high-symmetry lines in the Brillouin zone[73] in Figure 8. The calculations are in good agreement with experiment, especially in the longitudinal acoustic mode and the optical modes. This suggests that the harmonic approximation of APL is adequate, and we do not need to look at anharmonic effects in tin.

Price[72] and Rowe *et al.*[71] measured the phonon spectrum of  $\beta$ -Sn (white tin, *Strukturbericht* A5) at 300K and 296K, respectively. At this temperature the primitive cell volume is  $54.1\text{\AA}^3$ , so we compare with our calculations at  $54\text{\AA}^3$ . The results are shown in Figure 9. The agreement with experiment is not as quite as good as in  $\alpha$ -Sn, but the overall agreement is adequate.

There are no samples of simple hexagonal (*Strukturbericht* A<sub>7</sub>) tin, but alloying with indium is known to stabilize this phase. Ivanov *et al.*[10] measured the phonon

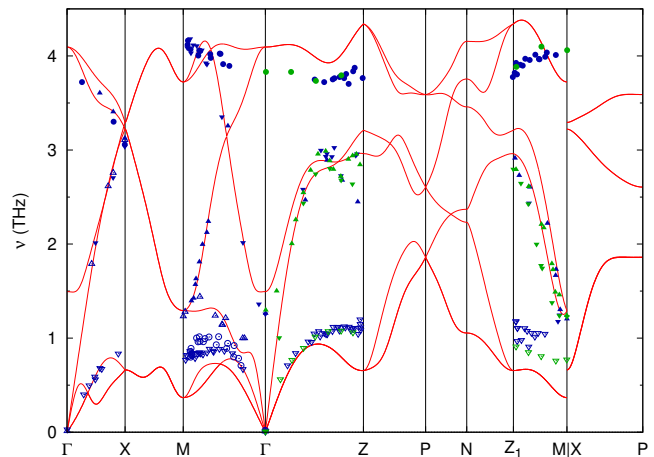


FIG. 9: Transverse (open symbols) and longitudinal (closed symbols) phonon frequencies for  $\beta$ -Sn measured at 300K by Price[72] (blue symbols) and Rowe *et al.*[71] at 296K (green symbols) compared to the PBE phonon spectra at the primitive cell volume of  $54\text{\AA}^3$  calculated using the APL module of AFLOW. The high-symmetry paths through the body-centered tetragonal Brillouin zone are defined by Setyawan and Curtarolo.[73] Note that Price only determined the frequencies of one acoustic and one optic transverse branch along the  $\Gamma - X$  ( $\Delta$ ) line. Data points were obtained from the references using the Engauge Digitizer.[41]

spectrum of  $\gamma$ -Sn  $\text{Sn}_{0.8}\text{In}_{0.2}$  at room temperature, where they found the sample to have a primitive cell volume of  $26.8\text{\AA}^3$ . We compare that to our calculations for pure simple hexagonal tin at  $27\text{\AA}^3$  in Figure 10. Here the agreement is excellent.

As the figures show, the APL module can accurately predict the phonon frequencies of tin in all three phases. We can perform one more check on the accuracy of the APL by determining the thermal expansion coefficient for the  $\alpha$ - and  $\beta$ -Sn phases. We could not find data for the thermal expansion of  $\gamma$ -Sn, even as an alloy.

### B. Thermal Expansion

The APL module of AFLOW prints the vibrational free energy of at intervals of 10K, so we can easily find the minimum free-energy volume  $V(T)$  over a large number of points. To determine  $\alpha(T)$  we fit our data for  $V(T)$  to the Padé approximate

$$V(T) = \frac{V_0 + a_1T + a_2T^2 + a_3T^3}{1 + b_1T + b_2T^2}, \quad (6)$$

which fits the expected linear behavior of  $V(T)$  at high temperatures. From this we determine the linear expansion, averaged over all directions, using (5).

The thermal expansion of  $\alpha$ -Sn is shown in Figure 11. Above 200K  $\alpha(T)$  is approximately constant, tending toward a value of  $8.5 \times 10^{-6}$ . Below 100K our predictions

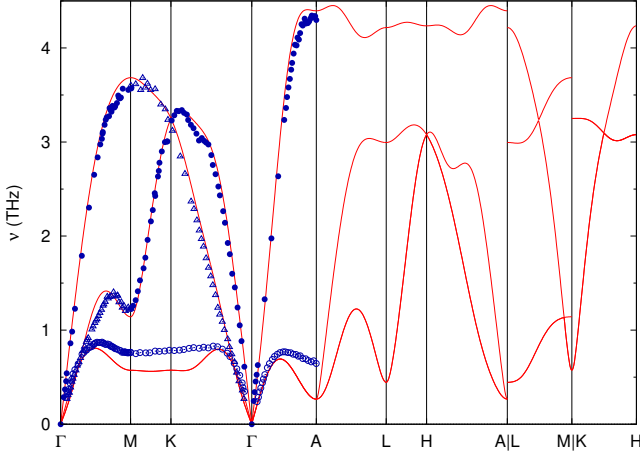


FIG. 10: Transverse (open symbols) and longitudinal (closed symbols) phonon frequencies for  $\gamma$ -Sn,  $\text{Sn}_{0.8}\text{In}_{0.2}$  at room temperature,[10] compared to the PBE phonon spectra at a primitive cell volume of  $27\text{\AA}^3$  calculated using the APL module of AFLOW. The high-symmetry paths through the simple hexagonal Brillouin zone are defined by Setyawan and Curtarolo.[73] Data points were obtained from the references using the Engauge Digitizer.[41]

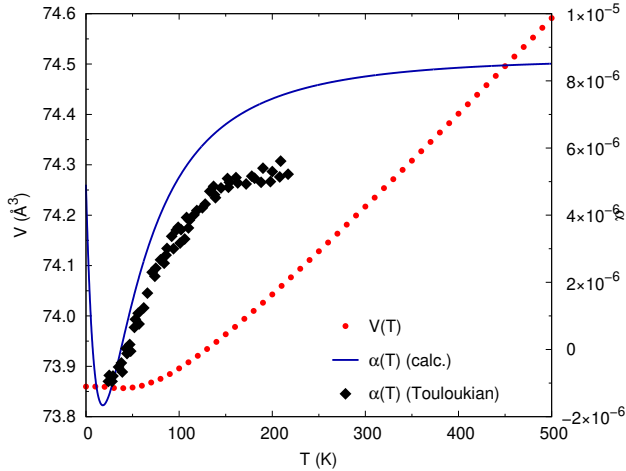


FIG. 11: The primitive-cell volume of  $\alpha$ -Sn as function of temperature (left axis, points), and linear expansion coefficient  $\alpha$  (right axis, line) calculated by APL using the PBE density functional. We also plot the experimental data found in Touloukian *et al.*[74] (black diamonds).

are in excellent agreement with the experimental data of Touloukian *et al.*,[74] although their curve flattens out at a lower value than ours.

$\beta$ -Sn has a tetragonal lattice, so the lattice parameters  $a(T)$  and  $c(T)$  can have different thermal expansion coefficients,

$$\alpha_{\parallel}(T) = \frac{1}{3a(T)} \frac{da}{dT}(T) \text{ and } \alpha_{\perp}(T) = \frac{1}{3c(T)} \frac{dc}{dT}(T), \quad (7)$$

where  $\parallel$  and  $\perp$  denote expansion in the  $a, b$  plane and

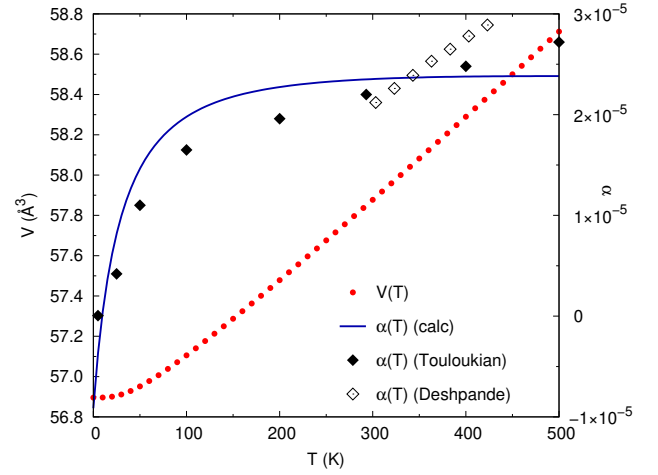


FIG. 12: The primitive-cell volume of  $\beta$ -Sn as function of temperature (left axis, points), and linear expansion coefficient  $\alpha$  (right axis, line) calculated by APL using the PBE density functional. We also plot the value of  $\alpha(T)$  found in Touloukian *et al.*,[74] (solid black diamonds) and measured by Deshpande and Sirdeshmukh[67] (open black diamonds).

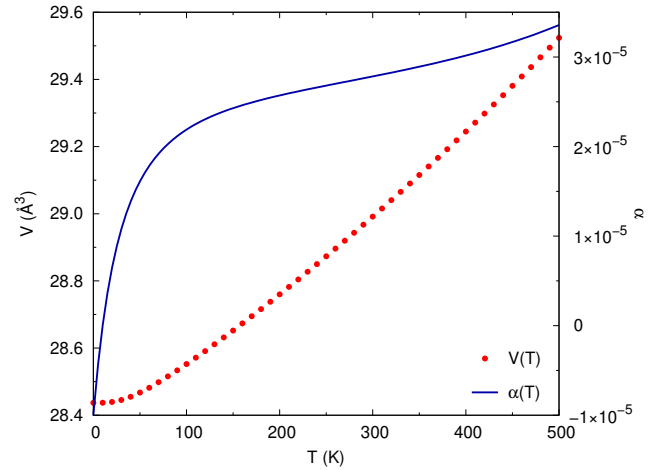


FIG. 13: The primitive-cell volume of  $\gamma$ -Sn as function of temperature (left axis, points), and linear expansion coefficient  $\alpha$  (right axis, line) calculated by APL using the PBE density functional.

along the  $c$  axis, respectively. The averaged thermal expansion is then

$$\alpha(T) = \frac{1}{3} [2\alpha_{\parallel}(T) + \alpha_{\perp}(T)] . \quad (8)$$

We compare predicted thermal expansion of  $\beta$ -Sn to the experimental data cited in Touloukian *et al.*,[74] (solid black diamonds) and measured by Deshpande and Sirdeshmukh[67] in Figure 12. We find good agreement with the experimental data, but note that the experimental value of  $\alpha$  is still increasing at 500K, where our prediction is that it remains constant above 300K.

There is no experimental information about the ther-

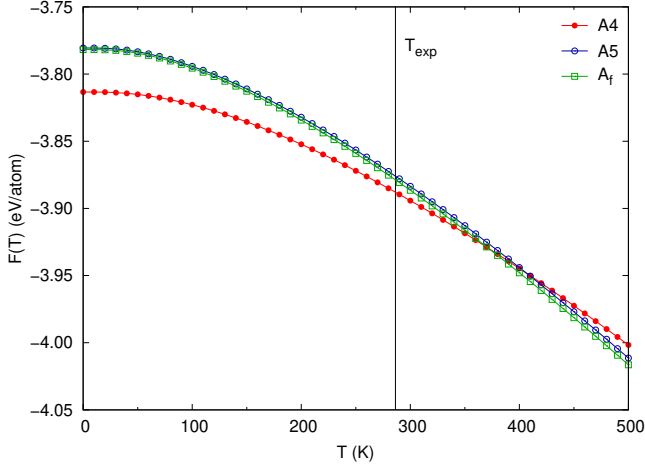


FIG. 14: Free energy as a function of temperature for  $\alpha$ -Sn (solid circles, *Strukturbericht* A4),  $\beta$ -Sn (open circles, *Strukturbericht* A5), and simple hexagonal  $\gamma$ -Sn (open squares, *Strukturbericht* A<sub>f</sub>). The vertical line shows the experimental  $\alpha$ - $\beta$  phase transition at 286K (13°C).[2]

mal expansion of  $\gamma$ -Sn or even  $\text{Sn}_{0.8}\text{In}_{0.2}$ , but we can determine the thermal expansion parameter, which we plot in Figure 13. We find that  $\alpha(T)$  is still increasing up to 500K, albeit not as rapidly as in experimental  $\beta$ -Sn. Around room temperature we find  $\alpha \approx 2.8 \times 10^{-5}$ , about 15% larger than in  $\beta$ -Sn.

### C. Thermal Phase Transitions

Now that we have shown that APL/AFLOW/VASP can compute both the phonon spectra and thermal expansion of tin, at least while using the PBE functional, we can turn to the question of phase stability: can we predict the transition from  $\alpha$ - to  $\beta$ -Sn, and is there a transition from  $\beta$ - to  $\gamma$ -Sn?

We have determined the free energy  $F(T)$  for all three phases using the PBE functional as outlined at the start of this section. The results are shown in Figure 14. We find that the  $\alpha$ - $\beta$  phase transition occurs at 400K, some distance from the experimental temperature of 286K,[2] but at least in the correct range. Unfortunately, the free energy of simple hexagonal  $\gamma$ -Sn is always lower than  $\beta$ -Sn, and we predict an  $\alpha$ - $\gamma$  transition at 370K. This is not particularly surprising given that static lattice calculations using PBE give  $U_\gamma$  lower than  $U_\beta$  at volumes (Figure 3) and the phonon frequencies of  $\beta$ -Sn (Figure 9) and  $\gamma$ -Sn (Figure 10) are spread over a comparable range of frequencies, suggesting that their thermal properties should be similar.

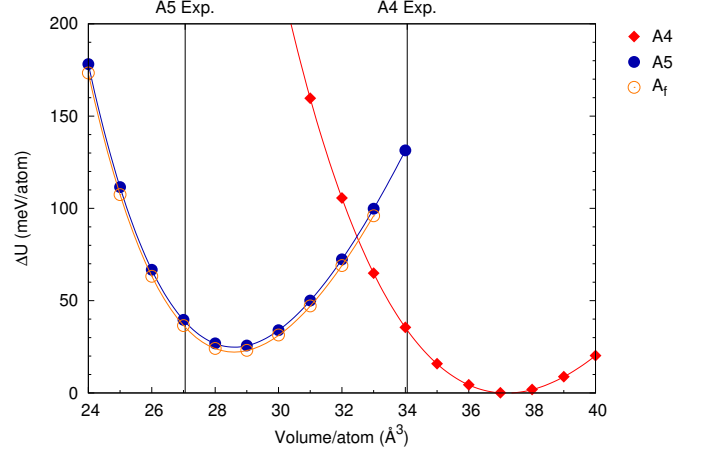


FIG. 15: Static lattice energy-volume curves for  $\alpha$ - (A4),  $\beta$ - (A5), and  $\gamma$ -Sn (A<sub>f</sub>), using LDA+U applied to the PBE functional with a shift  $U_p = 0.25$  eV. Since this is likely to predict a  $\alpha \rightarrow \gamma$  transition we did not pursue further calculations.

### D. The SCAN Functional

The SCAN functional correctly predicts the ordering  $U(\alpha\text{-Sn}) < U(\beta\text{-Sn}) < U(\gamma\text{-Sn})$  (Figure 7) so we expect that we will find the correct ordering of thermal phase transitions. The energy difference between the  $\alpha$ - and  $\beta$ -phases is approximately 80 meV/atom using SCAN, compared to 40 meV/atom using PBE, so that the predicted phase transitions will be much higher than the transitions found using PBE, which are already too large compared to experiment. Given this, and the cost of computing phonon frequencies using  $\approx 250$  atom supercells with a meta-GGA, we will not look at the phase transitions using the SCAN functional at this time.

## VI. OPTIMIZING DFT VIA COULOMB CORRECTIONS

Of course this work is not the first to study the  $\alpha$ - $\beta$  transition in tin, although it is the first to look in detail at the  $\gamma$ -Sn problem. Some time ago Pavone *al.*[13] found the  $\alpha$ - $\beta$  phase transition at 311K, in reasonable agreement with experiment, but probably influenced by errors in the LDA-based ultrasoft pseudopotentials.[75] Christensen and Methfessel found that they could adjust the energy difference between the  $\alpha$ - and  $\beta$ -phases by shifting the tin 4d orbitals within a full-potential Linearized Muffin-Tin Orbital scheme.[69] Legrain *et al.*[17] simply adjusted the  $\alpha$ - $\beta$  energy difference until the curves in Figure 14 crossed at the experimental transition temperature, and Legrain and Manzhos[18] showed that applying a Hubbard U correction of 1 eV to the tin 4s orbital changes the energy difference from 40 meV to 23 meV, approximately what is needed to lower the transition tem-

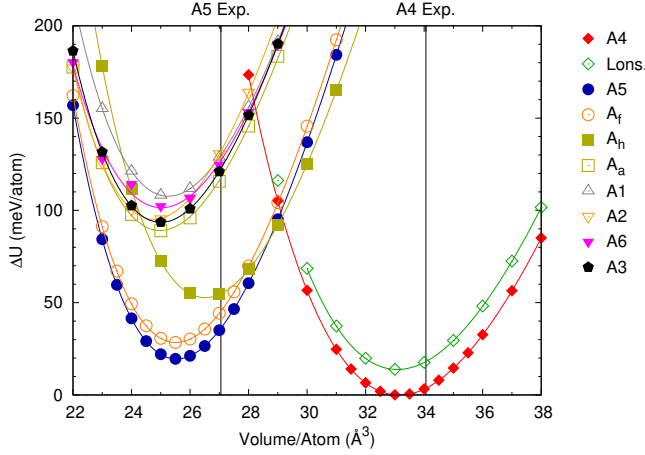


FIG. 16: Static lattice energy-volume curves for the tin structures discussed in Section III as predicted by AFLOW/VASP using the LDA functional with a Hubbard correction  $U_p = -0.8$  eV. The notation is identical to that in Figure 2.

perature to the experimental value.

This last work led us to investigate the effect of a Hubbard  $U$  correction on the  $\alpha$ - $\beta$  transition with VASP.[32] VASP allows us to apply the Hubbard  $U$  to a single orbital for each atomic species in the calculation. We chose to shift the  $p$  orbitals using the LDSA+ $U$  scheme of Liechtenstein.[76] This is purely a variational parameter, as we do not have a physical reason for doing this except the expectation that we can change the relative energies of these systems. We experimented with the choice of  $U$  in order to shift the  $\alpha$ - $\beta$  energy difference to approximately 20 meV, which should give us a transition temperature on the order of experiment.

We first tried this technique with the PBE functional, which would seem to need the smallest correction. If we take a value for  $U_p = 0.25$  eV, we lower the equilibrium  $\alpha$ - $\beta$  energy difference to approximately 25 meV/atom, as shown in Figure 15. This does not change the relative order of the phases, and so it will still predict a phase transformation from  $\alpha$ -Sn to  $\gamma$ -Sn rather than to  $\beta$ -Sn.

We then tried the same technique using the LDA functional. If we apply a shift  $U_p = -0.8$  eV, we get the results shown in Figure 16. This is much more promising. The  $\alpha$ - $\beta$  energy difference is now 18 meV, and the  $\gamma$ -Sn phase is above the  $\beta$ -phase for all volumes studied. In fact the energy difference between  $\beta$ - and  $\gamma$ -Sn phase is large enough so that the barrier between the two phases vanishes. Frozen-phonon calculations using FROZSL from the ISOTROPY software Suite[40] show that the  $L_3^-$  phonon has an imaginary frequency. This instability is exactly what is required to transform the simple hexagonal structure to  $\beta$ -Sn,[46] and the frozen-phonon supercells produced by FROZSL indeed relax to  $\beta$ -Sn.

We can look at the thermal expansion in both  $\alpha$ - (Fig-

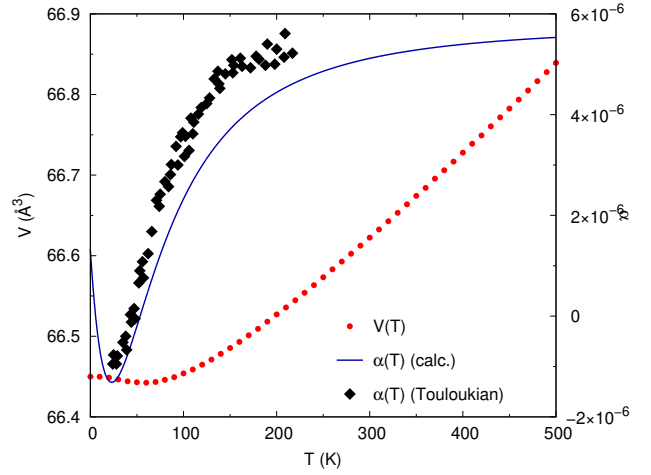


FIG. 17: The primitive-cell volume of  $\alpha$ -Sn as function of temperature (left axis, points), and linear expansion coefficient  $\alpha$  (right axis, line) calculated by APL using LDAU with  $U_p = -0.8$  eV. We also plot the experimental data found in Touloukian *et al.*[74] (black diamonds).

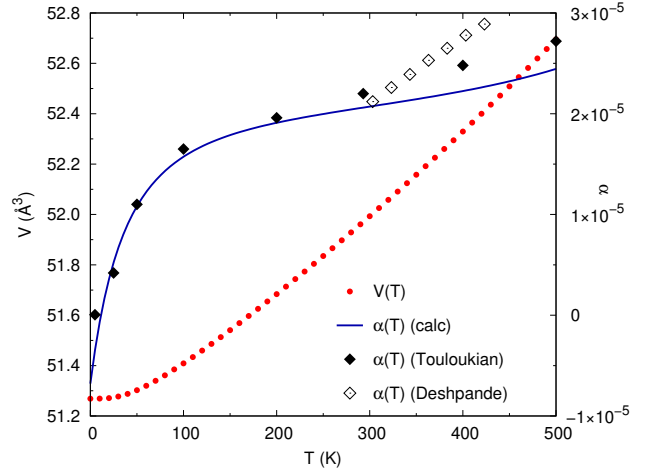


FIG. 18: The primitive-cell volume of  $\beta$ -Sn as function of temperature (left axis, points), and linear expansion coefficient  $\alpha$  (right axis, line) calculated by APL using the LDAU with  $U_p = -0.8$  eV. We also plot the value of  $\alpha(T)$  found in Touloukian *et al.*,[74] (solid black diamonds) and measured by Deshpande and Sirdeshmukh[67] (open black diamonds).

ure 17) and  $\beta$ -Sn (Figure 18). In both cases the thermal expansion is somewhat smaller than found using the PBE. Our prediction for  $\alpha(T)$  for  $\alpha$ -Sn is slightly smaller than experiment, but in  $\beta$ -Sn we find excellent agreement with experiment up to room temperature.

The thermal phase transition is again computed by the procedure outlined in Section V, but this time we using the LDA and  $U_p = -0.8$  eV, obtaining the free energies shown in Figure 19. Now the transition is predicted to occur at 245K. With further adjustment of  $U_p$  we can obviously shift the curves so that the transition is at the experimental value of 286K.

TABLE III: Effect of changing the kinetic energy cutoff and k-point mesh density on the equilibrium properties of  $\alpha$ -,  $\beta$ -, and  $\gamma$ -Sn, for the LDA, PBE, and SCAN functionals used in VASP. The left-hand column under each functional uses the AFLOW default kinetic energy cutoff (ENMAX) and k-point mesh (KMESH), while the right-hand column uses a higher energy cutoff and denser k-point mesh, as shown. Equilibrium volume ( $V_0$ ) and  $c/a$  ratios are computed from the final configuration found by VASP. The volume  $V_0$  is the volume of the primitive cell for each atom, but the energy differences are per atom.

	LDA		PBE		SCAN	
ENMAX	144.6	350.0	144.6	350.0	337.5	725.0
$\alpha$ -Sn Equilibrium Configuration						
KMESH	$16 \times 16 \times 16$	$24 \times 24 \times 24$	$16 \times 16 \times 16$	$24 \times 24 \times 24$	$16 \times 16 \times 16$	$24 \times 24 \times 24$
$V_0$ ( $\text{\AA}^3$ )	67.98413	67.95582	73.62472	73.58994	69.67733	70.64511
$\beta$ -Sn Equilibrium Configuration						
KMESH	$24 \times 24 \times 24$	$32 \times 32 \times 32$	$24 \times 24 \times 24$	$32 \times 32 \times 32$	$24 \times 24 \times 24$	$32 \times 32 \times 32$
$V_0$ ( $\text{\AA}^3$ )	52.36742	52.39377	56.64443	56.69880	54.39482	55.08161
$c/a$	0.54174	0.54117	0.54186	0.54175	0.54111	0.53850
$\gamma$ -Sn Equilibrium Configuration						
KMESH	$21 \times 21 \times 19$	$36 \times 36 \times 36$	$21 \times 21 \times 19$	$36 \times 36 \times 36$	$21 \times 21 \times 19$	$36 \times 36 \times 36$
$V_0$ ( $\text{\AA}^3$ )	26.16382	26.19763	28.33760	28.35201	27.13348	27.48595
$c/a$	0.93782	0.93825	0.93969	0.93982	0.93832	0.93818
Equilibrium Energy Differences (eV/atom)						
$U(\beta\text{-Sn}) - U(\alpha\text{-Sn})$	-0.02309	-0.02324	0.03961	0.03856	0.08123	0.07261
$U(\gamma\text{-Sn}) - U(\alpha\text{-Sn})$	-0.02101	-0.02041	0.03913	0.03840	0.08573	0.08001
$U(\gamma\text{-Sn}) - U(\beta\text{-Sn})$	0.00208	0.00284	-0.00048	-0.00015	0.00450	0.00740

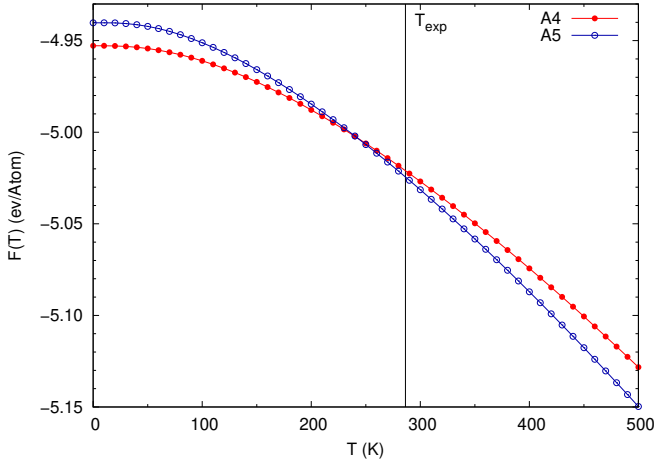


FIG. 19: Free energy as a function of temperature for  $\alpha$ -Sn (solid circles, *Strukturbericht* A4) and  $\beta$ -Sn (open circles, *Strukturbericht* A5), using the LDAU a Hubbard shift  $U_p = -0.8$  eV. The vertical line shows the experimental  $\alpha$ - $\beta$  phase transition at 286K (13°C).[2]

## VII. HIGH-THROUGHPUT CALCULATIONS AND CONVERGENCE

By their nature, high-throughput calculations rely on a set of standard assumptions, in particular that the basis set size (kinetic energy cutoff in a plane-wave code) and k-point mesh can be fixed without regard to the crystal structure being studied. For example, by de-

fault AFLOW sets the kinetic energy cutoff (ENMAX in VASP) to 140% of the minimum value recommended by VASP and the k-point mesh to give a minimum of 8000 k-points per reciprocal atom in the Brillouin zone,[77] equivalent to a  $20 \times 20 \times 20$  k-point mesh for a cubic system. While these standard values are usually sufficient, they may lead to errors when energy differences between phases are small.

We tested the reliability of the default energy cutoff and k-point size for tin by performing two sets of calculations to find the minimum energy configuration for the  $\alpha$ -,  $\beta$ -, and  $\gamma$ -Sn phases. The first set used the AFLOW default values for both quantities. The second set approximately doubled the energy cutoff, and increased the k-point density in the Brillouin zone. The results are shown in Table III. There is little difference between the two calculations' equilibrium volumes and  $c/a$ . There is a larger discrepancy in the energy differences. In the LDA the change can be as much as 0.6 meV, while in SCAN the change is as much as 3 meV. Fortunately this does not change the overall conclusions of the preceding sections.

For an even more extreme example of the importance of energy cutoffs and k-point meshes, consider the energy barrier along the Needs-Martin path (4): compute the barrier between  $\beta$ - and  $\gamma$ -Sn by fixing  $z$  and allowing VASP to relax the orthorhombic cell's lattice constants. Starting positions for the orthorhombic lattice for each  $z$  value are linearly interpolated from the end points. We did this calculation with the PBE functional with "quick" settings of ENMAX = 144.6 eV and



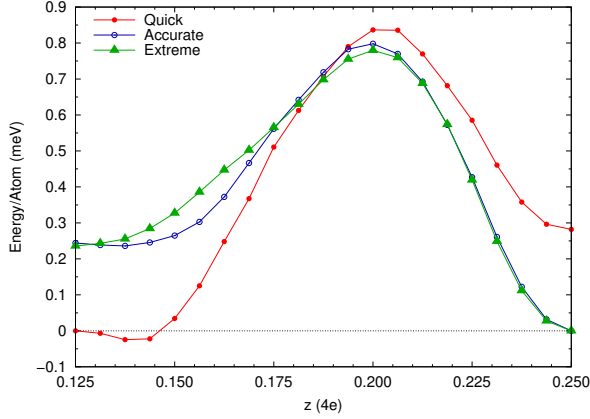


FIG. 20: (color online) Energy barrier for the path from  $\beta$ -Sn to  $\gamma$ -Sn from Needs and Martin[46] (4). The closed-circle red symbols are from the “quick” calculations, the open blue symbols are from the “accurate” calculations, and the green triangles from the “extreme” calculations described in the text. The energy differences between the end-point phases shown here differ from those in Table II because we have not reached convergence in the k-point mesh, and the unit cells and k-point meshes used to describe the  $\gamma$ -Sn phase differ in the two cases.

KMESH= $32 \times 32 \times 32$  (4504 k-points in the irreducible Brillouin zone); with the “accurate” settings, ENMAX = 350 eV and KMESH= $36 \times 36 \times 36$  (6346 k-points); and an “extreme” k-point mesh, ENMAX = 350 eV and KMESH= $48 \times 48 \times 48$  (14,725 k-points). The results are shown in Figure 20.

Here we find that the lowest energy structure shifts from the quick to the accurate cases, and that the energy difference between the structures does not agree with what we found in Table III even in the “accurate” or “extreme” cases. This is because the k-point meshes we use, while adequate for  $\beta$ -Sn structure, are far from ideal for the hexagonal lattice of the  $\gamma$ -Sn structure. The smaller k-point meshes do not predict the correct behavior for small distortions away from the  $\beta$ -Sn structure, predicting that the  $\beta$ -Sn phase is not even metastable within the PBE. This instability would correspond to an imaginary transverse acoustic phonon near  $\Gamma$  in Figure 9. The stability of the  $\beta$ -Sn phase can only be confirmed with the denser k-point mesh.

## VIII. SUMMARY

We used first-principles density functional calculations to study the  $\alpha$ -Sn  $\rightarrow$   $\beta$ -Sn phase transition and the pos-

sible transition to a hexagonal  $\gamma$ -Sn phase using a variety of density functionals available in VASP within the AFLOW high-throughput framework. The SCAN functional is the only one which predicts the correct sequence,  $U(\alpha\text{-Sn}) < U(\beta\text{-Sn}) < U(\gamma\text{-Sn})$ , and there the energy difference  $U(\beta\text{-Sn}) - U(\alpha\text{-Sn})$  is much too large to account for the low temperature of the phase transition. The only other functional which predicts the  $\beta$ -Sn phase to be above  $\alpha$ -Sn is PBE, but it orders the functions so that  $U(\alpha\text{-Sn}) < U(\gamma\text{-Sn}) < U(\beta\text{-Sn})$ . If we ignore the  $\gamma$ -Sn phase we get the  $\alpha \rightarrow \beta$  transition at 400K, some 120K above experiment. Of the remaining functionals, the LDA and other GGA functionals all predict the  $\beta$  phase to be the ground state of tin, and the non-SCAN meta-GGAs predict that the hexagonal close-packed phase is the ground state, and indeed overbind all of the close-packed phases.

We used a Hubbard  $U$  Coulomb correction as a fitting parameter, and found that we can adjust the value of  $U_p$  so that we can get the  $\alpha$ - $\beta$  energy difference needed to get the phase transition near 286K. Applying a Hubbard  $U$  to the PBE functional still leaves the  $\gamma$ -Sn phase lower in energy than  $\beta$ -Sn, but a correction to the LDA will get us to the correct transition temperature, and the  $\gamma$ -Sn phase is unstable and relaxes to  $\beta$ -Sn. Whether this last finding is correct or not depends on the existence of the hexagonal or near-hexagonal  $\gamma$ -Sn phase described by Kubiak.[8]

We have also looked to see if our predictions change when we use basis-set sizes and k-point meshes larger than the AFLOW default. We find that our overall predictions do not change, but care must be taken if very accurate results are desired.

In conclusion, none of the tested density functionals actually predict the proper behavior of tin, making this system an ideal test for the evaluation of new functionals.

## Acknowledgments

The authors thank Ohad Levy and Cormac Toher for valuable discussions. This work has been supported by ONR Grants N00014-20-1-2525 and N00014-20-1-2200. R.F. acknowledges support from the Alexander von Humboldt foundation under the Feodor Lynen research fellowship. Some calculations were performed on the United States Naval Academy Cray, Grace.

[1] M. J. Mehl, D. Hicks, C. Toher, O. Levy, R. M. Hanson, G. Hart, and S. Curtarolo, *The AFLOW Library of Crystallographic Prototypes: Part 1*, Computational Ma-

terials Science **136**, S1–S828 (2017).

[2] E. Cohen and A. K. W. A. van Lieshout, *Physikalisch-chemische Studien am Zinn. X. Die Umwandlungstem-*

- peratur graues Zinn  $\rightleftharpoons$  weisses Zinn, Zeitschrift für Physikalische Chemie A **173**, 32–34 (1935).
- [3] B. Cornelius, S. Treivish, Y. Rosenthal, and M. Pecht, *The phenomenon of tin pest: A review*, Microelectronics Reliability **79**, 175–192 (2017).
  - [4] J. Fritzsche, *Ueber eigenthülich modificirtes Zinn*, Berichte der deutschen chemischen Gesellschaft pp. 112–113 (1869).
  - [5] W. J. Plumbridge, *Tin pest issues in lead-free electronic solders*, Journal of Materials Science: Materials in Electronics **18**, 307–318 (2007).
  - [6] P. L. Couteur and J. Burreson, *Napoleon's Buttons: How 17 Molecules Changed History* (Tarcher Perigee, New York, 2004).
  - [7] R. Pfister and P. Pugnât, *Tin Pest: A Forgotten Issue in the Field of Applied Superconductivity?* (2012). arXiv:1204.1443 [cond-mat.supr-con].
  - [8] R. Kubiak, *Evidence for the existence of the  $\gamma$  form of tin*, Journal of the Less Common Metals **116**, 307–311 (1986).
  - [9] R. H. Kane, B. C. Giessen, and N. J. Grant, *New metastable phases in binary tin alloy systems*, Acta Metallurgica **14**, 605–609 (1966).
  - [10] A. S. Ivanov, A. Y. Rumiantsev, B. Dorner, N. L. Mitrofanov, and V. V. Pushkarev, *Lattice dynamics and electron-phonon interaction in  $\gamma$ -tin*, Journal of Physics F: Metal Physics **17**, 1925–1934 (1987).
  - [11] A. S. Ivanov, A. Y. Rumiantsev, N. L. Mitrofanov, and M. Alba, *Low-frequency lattice dynamics of  $\gamma$ -tin*, Physica B: Condensed Matter **174**, 79–82 (1974).
  - [12] E. Parthé, L. Gelato, B. Chabot, M. Penso, K. Cen-zula, and R. Gladyshevskii, *Standardized Data and Crystal Chemical Characterization of Inorganic Structure Types*, Gmelin Handbook of Inorganic and Organometallic Chemistry, vol. 2 (Springer-Verlag, Berlin, Heidelberg, 1993), 8 edn.
  - [13] P. Pavone, S. Baroni, and S. de Gironcoli,  *$\alpha \leftrightarrow \beta$  phase transition in tin: A theoretical study based on density-functional perturbation theory*, Physical Review B **1998**, 10421–10423 (57).
  - [14] K. Houben, J. K. Jochum, D. P. Lozano, M. Bisht, E. Menéndez, D. G. Merkel, R. Rüffer, A. I. Chumakov, S. Roelants, B. Partoens, M. V. Milošević, F. M. Peeters, S. Couet, A. Vantomme, K. Temst, and M. J. V. Bael, *In situ study of the  $\alpha$ -Sn to  $\beta$ -Sn phase transition in low-dimensional systems: Phonon behavior and thermodynamic properties*, Physical Review B **100**, 075408 (2019).
  - [15] J. Ihm and M. L. Cohen, *Equilibrium properties and the phase transition of grey and white tin*, Physical Review B **23**, 1576–1579 (1981).
  - [16] S.-H. Na and C.-H. Park, *First-Principles Study of the Structural Phase Transition in Sn*, Journal of the Korean Physical Society **56**, 494–497 (2010).
  - [17] F. Legrain, O. I. Malyi, C. Persson, and S. Manzhos, *Comparison of alpha and beta tin for lithium, sodium, and magnesium storage: An ab initio study including phonon contributions*, Journal of Chemical Physics **143**, 204704 (2015).
  - [18] F. Legrain and S. Manzhos, *Understanding the difference in cohesive energies between alpha and beta tin in DFT calculations*, AIP Advances **6**, 045116 (2016).
  - [19] S. Curtarolo, W. Setyawan, G. L. W. Hart, M. Jahnátek, R. V. Chepulskii, R. H. Taylor, S. Wang, J. Xue, K. Yang, O. Levy, M. J. Mehl, H. T. Stokes, D. O. Demchenko, and D. Morgan, *AFLOW: An automatic framework for high-throughput materials discovery*, Computational Materials Science **58**, 218–226 (2012).
  - [20] C. Toher, C. Oses, D. Hicks, E. Gossett, F. Rose, P. Nath, D. Usanmaz, D. C. Ford, E. Perim, C. E. Calderon, J. J. Plata, Y. Lederer, M. Jahnátek, W. Setyawan, S. Wang, J. Xue, K. Rasch, R. V. Chepulskii, R. H. Taylor, G. Gomez, H. Shi, A. R. Supka, R. A. R. A. Orabi, P. Gopal, F. T. Cersoli, L. Liyanage, H. Wang, I. Siloi, L. A. Agapito, C. Nyshadham, G. L. W. Hart, J. Carrete, F. Legrain, N. Mingo, E. Zurek, O. Isayev, A. Tropsha, S. Sanvito, R. M. Hanson, I. Takeuchi, M. J. Mehl, A. N. Kolmogorov, K. Yang, P. D'Amico, A. Calzolari, M. Costa, R. D. Gennaro, M. B. Nardelli, M. Fornari, O. Levy, and S. Curtarolo, *The AFLOW Fleet for Materials Discovery*, in *Handbook of Materials Modeling*, edited by W. Andreoni and S. Yip (Springer International Publishing, Cham, Switzerland, 2018), pp. 1–28.
  - [21] C. Oses, C. Toher, and S. Curtarolo, *Data-driven design of inorganic materials with the Automatic Flow Framework for Materials Discovery*, MRS Bulletin **43**, 670–675 (2018).
  - [22] C. Nyshadham, C. Oses, J. E. Hansen, I. Takeuchi, S. Curtarolo, and G. L. W. Hart, *A computational high-throughput search for new ternary superalloys*, Acta Mater. **122**, 438–447 (2017).
  - [23] M. Jahnátek, O. Levy, G. L. W. Hart, L. J. Nelson, R. V. Chepulskii, J. Xue, and S. Curtarolo, *Ordered phases in ruthenium binary alloys from high-throughput first-principles calculations*, Phys. Rev. B **84**, 214110 (2011).
  - [24] Y. Lederer, C. Toher, K. S. Vecchio, and S. Curtarolo, *The search for high entropy alloys: A high-throughput ab-initio approach*, Acta Mater. **159**, 364–383 (2018).
  - [25] G. Kresse and J. Hafner, *Ab initio molecular dynamics for liquid metals*, Physical Review B **47**, 558–561 (1993).
  - [26] G. Kresse and J. Hafner, *Ab initio molecular-dynamics simulation of the liquid-metal-amorphous-semiconductor transition in germanium*, Physical Review B **49**, 14251–14269 (1994).
  - [27] G. Kresse and J. Furthmüller, *Efficiency of ab-initio total energy calculations for metals and semiconductors using a plane-wave basis set*, Computational Materials Science **6**, 15–50 (1996).
  - [28] G. Kresse and J. Furthmüller, *Efficient iterative schemes for ab initio total-energy calculations using a plane-wave basis set*, Physical Review B **54**, 11169–11186 (1996).
  - [29] S. Curtarolo, W. Setyawan, G. L. W. Hart, M. Jahnátek, R. V. Chepulskii, R. H. Taylor, S. Wang, J. Xue, K. Yang, O. Levy, M. J. Mehl, H. T. Stokes, D. O. Demchenko, and D. Morgan, *AFLOW: An automatic framework for high-throughput materials discovery*, Comput. Mater. Sci. **58**, 218–226 (2012).
  - [30] J. J. Plata, P. Nath, D. Usanmaz, J. Carrete, C. Toher, M. de Jong, M. D. Asta, M. Fornari, M. Buongiorno Nardelli, and S. Curtarolo, *An efficient and accurate framework for calculating lattice thermal conductivity of solids: AFLOW-AAPL Automatic Anharmonic Phonon Library*, npj Comput. Mater. **3**, 45 (2017).
  - [31] M. J. Mehl, D. Finkenstadt, C. Dane, G. L. W. Hart, and S. Curtarolo, *Finding the stable structures of  $N_{1-x}W_x$  with an ab initio high-throughput approach*, Physical Review B **91**, 184100 (2015).
  - [32] O. Bengone, M. Alouani, P. Blöchl, and J. Hugel, *Implementation of the projector augmented-wave LDA+U*



- method: Application to the electronic structure of NiO, *Physical Review B* **62**, 16392 (2000).
- [33] A. Rohrbach, J. Hafner, and G. Kresse, *Electronic correlation effects in transition-metal sulfides*, *Journal of Physics: Condensed Matter* **15**, 979–996 (2003).
  - [34] P. E. Blöchl, *Projector augmented-wave method*, *Physical Review B* **50**, 17953–17979 (1994).
  - [35] G. Kresse and D. Joubert, *From ultrasoft pseudopotentials to the projector augmented-wave method*, *Physical Review B* **59**, 1758–1725 (1999). 10.1103/PhysRevB.59.1758.
  - [36] J. P. Perdew, K. Burke, and M. Ernzerhof, *Generalized Gradient Approximation Made Simple*, *Physical Review Letters* **77**, 3865–3868 (1996).
  - [37] F. Birch, *Finite strain isotherm and velocities for single-crystal and polycrystalline nacl at high-pressures and 300-degree-k*, *Journal of Geophysical Research* **83**, 1257–1268 (1978).
  - [38] M. J. Mehl, *Pressure dependence of the elastic moduli in aluminum-rich Al-Li compounds*, *Physical Review B* **47**, 2493–2500 (1993).
  - [39] R. M. Hanson, J. Prilusky, Z. Renjian, T. Nakane, and J. L. Sussman, *Jmol*. An open-source Java viewer for chemical structures in 3D.
  - [40] H. T. Stokes, D. M. Hatch, and i. B. J. Campbell, *FROZSL*. ISOTROPY Software Suite.
  - [41] M. Mitchell, *Engauge Digitizer* (2019). Open source software, version 12.
  - [42] P. P. Ewald, C. Hermann, O. Lohrmann, H. Philipp, C. Gottfried, F. Schossberger, and K. Herrmann, eds., *Strukturbericht*, vol. I–VII (Akademische Verlagsgesellschaft M. B. H., 1937–1943).
  - [43] C. J. Smithells, *Metals Reference Book* (Butterworths Scientific, London, 1955), second edn.
  - [44] A. Yoshiasa, Y. Murai, O. Ohtaka, and T. Katsura, *Detailed Structures of Hexagonal Diamond (lonsdaleite) and Wurtzite-type BN*, *Japanese Journal of Applied Physics* **42**, 1694–1704 (2003).
  - [45] D. Hicks, M. J. Mehl, E. Gossett, C. Toher, O. Levy, R. M. Hanson, G. Hart, and S. Curtarolo, *The AFLOW Library of Crystallographic Prototypes: Part 2*, *Computational Materials Science* **161**, S1–S1011 (2019).
  - [46] R. J. Needs and R. M. Martin, *Transition from  $\beta$ -Sn to simple hexagonal silicon under pressure*, *Physical Review B* **30**, 5390–5392 (1984).
  - [47] G. V. Raynor and J. A. Lee, *The tin-rich intermediate phases in the alloys of tin with cadmium, indium and mercury*, *Acta Metallurgica* **2**, 616–620 (1954).
  - [48] G. J. Ackland, *High-pressure phases of group IV and III–V semiconductors*, *Reports on Progress in Physics* **64**, 483–516 (2001).
  - [49] B. Wehinger, A. Bosak, G. Piccolboni, K. Refson, D. Chernyshov, A. Ivanov, A. Rumiantsev, and M. Krisch, *Diffuse scattering in metallic tin polymorphs*, *Journal of Physics: Condensed Matter* **26**, 115401 (2014).
  - [50] N. G. Hörmann, A. Gross, J. Rohrer, and P. Kaghazchi, *Stabilization of the  $\gamma$ -Sn phase in tin nanoparticles and nanowires*, *Applied Physics Letters* **107**, 123101 (2015).
  - [51] L. Hedin and B. I. Lundqvist, *Explicit local exchange-correlation potentials*, *Journal of Physics C: Solid State Physics* **4**, 2064–2083 (1971).
  - [52] D. M. Ceperley and B. J. Alder, *Ground State of the Electron Gas by a Stochastic Method*, *Physical Review Letters* **45**, 566–569 (1980).
  - [53] J. P. Perdew and A. Zunger, *Self-interaction correction to density-functional approximations for many-electron systems*, *Physical Review B* **23**, 5048–5079 (1981).
  - [54] W. Kohn and L. J. Sham, *Self-Consistent Equations Including Exchange and Correlation Effects*, *Physical Review* **140**, A1133–A1138 (1965).
  - [55] J. P. Perdew, A. Ruzsinszky, G. I. Csonka, O. A. Vydrov, G. E. Scuseria, L. A. Constantin, X. Zhou, and K. Burke, *Restoring the Density-Gradient Expansion for Exchange in Solids and Surfaces*, *Physical Review Letters* **100**, 136406 (2008).
  - [56] R. Armiento and A. E. Mattsson, *Functional designed to include surface effects in self-consistent density functional theory*, *Physical Review B* **72**, 085108 (2005).
  - [57] A. E. Mattsson, R. Armiento, J. Paier, G. Kresse, J. M. Wills, and T. R. Mattsson, *The AM05 density functional applied to solids*, *Journal of Chemical Physics* **128**, 084714 (2008).
  - [58] J. Tao, J. P. Perdew, V. N. Staroverov, and G. E. Scuseria, *Climbing the Density Functional Ladder: Nonempirical Meta-Generalized Gradient Approximation Designed for Molecules and Solids*, *Physical Review Letters* **91**, 146401 (2003).
  - [59] J. P. Perdew, A. Ruzsinszky, G. I. Csonka, L. A. Constantin, and J. Sun, *Workhorse Semilocal Density Functional for Condensed Matter Physics and Quantum Chemistry*, *Physical Review Letters* **103**, 026403 (2009).
  - [60] J. Sun, B. Xiao, and A. Ruzsinszky, *Communication: Effect of the orbital-overlap dependence in the meta-generalized gradient approximation*, *Journal of Chemical Physics* **137**, 051101 (2012).
  - [61] J. Sun, R. Haunschild, B. Xiao, I. W. Bulik, G. E. Scuseria, and J. P. Perdew, *Semilocal and hybrid meta-generalized gradient approximations based on the understanding of the kinetic-energy-density dependence*, *Journal of Chemical Physics* **138**, 044113 (2013).
  - [62] Y. Zhao and D. G. Truhlar, *A new local density functional for main-group thermochemistry, transition metal bonding, thermochemical kinetics, and noncovalent interactions*, *Journal of Chemical Physics* **125**, 194101 (2006).
  - [63] J. Sun, A. Ruzsinszky, and J. Perdew, *Strongly Constrained and Appropriately Normed Semilocal Density Functional*, *Physical Review Letters* **115**, 036402 (2015).
  - [64] J. Sun, R. C. Remsing, Y. Zhang, Z. Sun, A. Ruzsinszky, H. Peng, Z. Yang, A. Paul, U. Waghmare, X. Wu, M. L. Klein, and J. P. Perdew, *Accurate first-principles structures and energies of diversely bonded systems from an efficient density functional*, *Nature Chemistry* **8**, 831–836 (2016).
  - [65] G. I. Csonka, J. P. Perdew, A. Ruzsinszky, P. H. T. Philipsen, S. Lebègue, J. Paier, O. A. Vydrov, and J. G. Ángyán, *Assessing the performance of recent density functionals for bulk solids*, *Physical Review B* **79**, 155107 (2009).
  - [66] J. Sun, M. Marsman, G. I. Csonka, A. Ruzsinszky, P. Hao, Y.-S. Kim, G. Kresse, and J. P. Perdew, *Self-consistent meta-generalized gradient approximation within the projector-augmented-wave method*, *Physical Review B* **84**, 035117 (2011).
  - [67] V. T. Deshpande and D. B. Sirdeshmukh, *Thermal Expansion of Tetragonal Tin*, *Acta Crystallographica* **14**, 355–356 (1961).
  - [68] D. L. Price, J. M. Rowe, and R. M. Nicklow, *Lattice*

- Dynamics of Grey Tin and Indium Antimonide*, Physical Review B **3**, 1268–1279 (1971).
- [69] N. E. Christensen and M. Methfessel, *Density-functional calculations of the structural properties of tin under pressure*, Physical Review B **48**, 5797–5807 (1993).
- [70] H. Olijnyk and W. B. Holzapfel, *Phase Transitions in Si, Ge and Sn Under Pressure*, Supplément au Journal de Physique Colloques **45**, 153–156 (1984).
- [71] J. M. Rowe, B. N. Brockhouse, and E. C. Svensson, *Lattice Dynamics of White Tin*, Physical Review Letters **14**, 554–556 (1965).
- [72] D. L. Price, *Lattice Dynamics of White Tin*, Proceedings of the Royal Society of London. Series A, Mathematical and Physical Sciences **300**, 25–44 (1967).
- [73] W. Setyawan and S. Curtarolo, *High-throughput electronic band structure calculations: Challenges and tools*, Computational Materials Science **49**, 299–312 (2010).
- [74] Y. S. Touloukian, R. K. Kirby, R. E. Taylor, and P. D. Desai, *Thermal Expansion Metallic Elements and Alloys* (New York : IFI/Plenum, 1975), *Thermophysical Properties of Matter - the TPRC Data Series*, vol. 12, pp. 339–345.
- [75] G. B. Bachelet, D. R. Hamann, and M. Schlüter, *Pseudopotentials that work: From H to Pu*, Physical Review B **26**, 4199–4228 (1982).
- [76] A. I. Liechtenstein, V. I. Anisimov, and J. Zaanen, *Density-functional theory and strong interactions: Orbital ordering in Mott-Hubbard insulators*, Physical Review B **52**, R5467–R5470 (1995).
- [77] C. E. Calderon, J. J. Plata, C. Toher, C. Oses, O. Levy, M. Fornari, A. Natan, M. J. Mehl, G. Hart, M. B. Nardelli, and S. Curtarolo, *The {AFLOW} standard for high-throughput materials science calculations*, Computational Materials Science **108**, Part A, 233–238 (2015).